

Simulation of Complex Cracking in Plain Weave C/SiC Composite under Biaxial Loading

RON-BIN CHENG AND SU-YUEN HSU

ABSTRACT: Finite element analysis is performed on a mesh, based on computed geometry of a plain weave C/SiC composite with assumed internal stacking, to reveal the pattern of internal damage due to biaxial normal cyclic loading. The simulation encompasses intertow matrix cracking, matrix cracking inside the tows, and separation at the tow-intertow matrix and tow-tow interfaces. All these dissipative behaviors are represented by traction-separation cohesive laws. Not aimed at quantitatively predicting the overall stress-strain relation, the simulation, however, does not take the actual process of fiber debonding into account. The fiber tows are represented by a simple rule-of-mixture model where the reinforcing phase is a hypothetical one-dimensional material. Numerical results indicate that for the plain weave C/SiC composite, 1) matrix-crack initiation sites are primarily determined by large intertow matrix voids and interlayer tow-tow contacts, 2) the pattern of internal damage strongly depends on the loading path and initial stress, 3) compressive loading inflicts virtually no damage evolution.

KEY WORDS: ceramic matrix composite, plain weave, cohesive model, brittle failure, smeared crack model, progressive damage, meso-mechanical analysis, finite element.

INTRODUCTION

Textile ceramic matrix composites (CMCs) have been proposed for thermal structures of reusable space vehicles, and high-temperature components of rocket engines and gas turbines. The state-of-the-art design methodology for such applications involves substantial conservatism because of the lack of homogeneous continuum models which can satisfactorily represent the pronounced loading history-dependent behavior of the composites, such as stress-strain relation, strength, and gas permeability. The loading-history dependence is a reflection of

Ron-Bin Cheng, Dassault Systèmes Simulia Corp., Warwick, RI.
Su-Yuen Hsu, NASA Langley Research Center, Hampton, VA.

widespread crack initiation, extension, closure, and opening in the composites.

Formulation of existing homogeneous continuum models for textile CMCs are mostly motivated by experience with isotropic materials (e.g., damage driven by positive strains), simplistic micromechanical or mesomechanical considerations (e.g., damage deactivation), or succinct mathematical generalization. Within the framework of thermodynamics, Chaboche and Maire [1], and Halm, Dragon, et. al. [2] developed continuum damage mechanics (CDM) models for textile CMCs by postulating the elastic stiffness tensor as a unified function of a 2nd-ranked tensorial damage variable and some scalar damage variables, and by postulating a damage potential as a function of the thermodynamic forces associated with the damage variables. As a result of the normality rule used to derive damage evolution equations and the convexity of the postulated damage potential, the second law of thermodynamics is satisfied. Camus [3] modeled degradation of compliance tensor components individually; thus, the second law of thermodynamics can be readily satisfied by proposing individual damage criteria and evolution equations. It seems that without a general internal physics-based rationale, the complexity of the anisotropic brittle material behavior of textile CMCs cannot be completely covered by the existing homogeneous continuum models. Detecting and tracking many simultaneous three-dimensional fractures in a textile CMC is extremely difficult, if not entirely impossible, during a mechanical test. Therefore, mesomechanical simulations, or numerical experiments, of the complex internal cracking may be performed to obtain knowledge that is useful for formulation of a homogeneous continuum model. In addition, material responses that are required for identification of material parameters of a homogeneous continuum model but are difficult to obtain from mechanical tests can be computed by mesomechanical simulation.

Substantial efforts focused on analyzing the response of unidirectional CMCs to longitudinal tensile loading by micromechanical approaches and yielded very instrumental results. An approximate closed-form nonsingular elastic stress distribution around a bridged matrix crack associated with a frictional fiber debonding zone in unidirectional CMCs under longitudinal tensile loading was derived from a shear-lag model in the classical work by Aveston and Kelly [4]. Curtin, Ahn, et al. [5] introduced into shear-lag analysis the number of flaws in a prismatic volume of matrix (or similarly in a fiber) that can propagate transversely throughout the material volume, as a function of applied axial stress, and the axial length and cross-sectional area of the material volume. In the analysis, the effect of fiber debonding on the stress field was evaluated by using fracture energy. Ismar and Streicher [6] performed finite element (FE) analysis of a unit cell of unidirectional SiC/SiC composites subject to longitudinal tensile loading, where element size-dependent strength probabilities are used to predict failure of the constituents and interfaces. Fiber cracks are assumed to be orthogonal to the fiber axis, while the orientation of matrix cracks is assumed to maximize the strain energy release rate. Elastic constants in a failed element are reduced according to

the orientation of the crack, and a maximum of three orthogonal cracks is allowed in each matrix element. Yang and Mall [7] developed a cohesive-shear-lag model, where the fiber follows a softening cohesive law in order to represent the average effect of the increasing number of broken fibers. Along the debonded interface, a slip zone and a stick zone, at most, may be present when the model is subject to cyclic loading. In the cohesive-shear-lag model, the matrix crack spacing is used for normalization of length dimension but does not need to be known when applying the model. Therefore, damage progression is represented by the normalized debonded length and reduced fiber stiffness, which in conjunction with two other model parameters were backed out from a low-cycle fatigue test on a SiC fiber-reinforced glass. It was shown in [7] that by using the backed-out parameters, stress-strain hysteresis loops were generated in good agreement with the experimental data for about ten thousand cycles. In general, the past work concerning longitudinal tensile loading indicated that consistency with fracture mechanics (or size-dependent failure) must be ensured in order to analyze damage progression in uniaxial CMCs at the microscopic level. In addition, fiber debonding and frictional sliding strongly influence the rate of decrease in matrix crack spacing as well as the hardening and hysteretic characteristics of the overall stress-strain response.

Mesomechanical analysis of textile CMCs has to cope with internal physical processes at the mesostructural level. Complicated interactions are present among the reinforcing fiber tows. They are arranged in an interlacing architecture, and most of the tows are in contact with some others. The interaction between matrix-rich regions and surrounding fiber tows is also critical because ceramic matrices, which usually play an important role (e.g., thermal protection) in CMC applications, may carry significant loads before they crack. Thus, one should expect complex progression of multiple cracks even in plain weave CMCs. As seen in the literature, the advancement in mesomechanical modeling of textile CMCs is very limited. Murthy, Mital, et al. [8] employed a computer code called W-CEMCAN to predict elastic, thermal expansion, and thermal conductivity properties of a five-harness satin weave SiC/SiC composite fabricated by chemical vapor infiltration (CVI). The code computes the effective behavior of the fiber tows in simplified micromechanical analysis, taking the fibers, matrix, and fiber coating into account, and then predicts the effective behavior of the fabric composite by treating a unit cell of the composite as an assembly of laminates. Sullivan, Murthy, et al. [9] backed out the respective in situ matrix moduli for a plain-weave C/SiC quasi-isotropic laminate and a three-dimensional (3-D) angle interlock woven C/SiC composite as nonlinear functions of stress and temperature by comparing properties predicted by W-CEMCAN with measured properties through a trial-and-error procedure. Afterwards, a full set of 3-D composite properties could be predicted and used in FE analysis of four-point bending of beams made of the composites. Kuhn, Haan, et al. [10] developed a multiscale approach to predicting nonlinear

response of CVI plain weave CMCs. The effective behavior of the fiber tows is computed by using the well-known Composite Cylinder Assembly model. The matrix, whether inside or outside the tows, is represented by a continuum damage mechanics model which has only one damage variable, standing for the microcrack density. The effective behavior of a plain weave composite is computed from a unit cell treated as a composite laminate with four nonuniform layers. Therefore, the mesomechanical problem is reduced to a two-dimensional problem, which is solved iteratively by the Rayleigh-Ritz method in [10]. From a theoretical standpoint, the approach developed in [10] is only suitable for the very early stage of material degradation, when there is no strain localization or mesocracks, such as cracks in matrix-rich regions or transverse cracks in the tows. Flores, Evans, et al. [11] developed an FE approach to predicting the effective stress-strain relation of CMCs with general fabric architecture. Line elements, assigned the longitudinal elastic stiffness of the fibers within a tow, are tied by multipoint constraint to solid elements, assigned nonlinear properties of an effective medium that complement the stiffness of the line elements and have to be calibrated. Thus, the effective medium properties are closely related to those of the matrix alone, but are not identical to them. The effects of matrix cracking, and interfacial debonding and sliding are also lumped into the effective medium behavior. As such, the effective medium should not be isotropic; however, an isotropic elastic-perfectly plastic model with the pressure-dependent Drucker-Prager yield criterion is chosen for the effective medium. It should be noted that due to the use of the smeared properties for the effective medium and the vanishing volume of the line elements, the resolution of the state of the matrix computed by the approach in [11] is only similar to that by the approach in [9].

An objective of this study is to reveal the pattern of damage in a CVI plain weave C/SiC composite subject to biaxial normal cyclic loading by FE mesomechanical analysis. The FE mesh is obtained from simulation of the in situ geometry, where tow-tow contact is ubiquitous. Four types of fracture, cracking in the matrix outside the fiber tows (intertow matrix), cracking in the matrix inside the fiber tows (simply called “tow matrix” below), tow-intertow matrix separation, and tow-tow separation, are computed in consideration of consistency with fracture mechanics. With the cracks computed, effects of large intertow matrix voids, tow-tow contact, initial stress, compressive loading, and loading history can be sifted.

Most physical quantities in the numerical examples are non-dimensional. Length is normalized by half the thickness of the plain weave under consideration, say, L . Quantities which have the same unit as stress are normalized by the longitudinal Young’s modulus of the fiber tows under consideration, say, σ . Therefore, energy dissipation per unit area of crack extension is normalized by σL .

COMPUTATIONAL MODEL

In the present study, all the computations are carried out on the finite element mesh shown in Figure 1 by the Abaqus/Explicit[®] program. The x and y axes of the rectangular coordinate system adopted for the analysis are aligned with the in-plane principal directions of the composite. The procedure for constructing the mesh is presented in detail in [12]. The internal geometry of the plain weave composite is obtained from a simplified simulation of the effects of interlacing and stacking. At the beginning of the simulation, each unconsolidated fiber tow is arranged along a piecewise linear path in a desired unit cell and pursuant to the fabric architecture. Moreover, the unconsolidated tows are assigned an idealized cross section with a reduced area so that the tows can be free of contact at the beginning. In the present study, identical fabric parameters are used for both principal directions, and the weaves are stacked up with perfect angular alignment and the maximum translational offset. A fictitious thermal expansion is then imposed on the transversely isotropic and elastic-ideally plastic tows to bring them into contact and their final shapes. By “growing” matrix on the fiber tows, a solid, which represents the intertow matrix volume and defines a large intertow matrix pore, is obtained (Figure 1). Large intertow pores are typically seen in CVI textile CMCs and are probable crack initiation sites [13]. The large intertow pore shown in Figure 1 converges to a small through hole at the center. Additional possible matrix-crack initiation sites, surmised from the geometry, are also shown in Figure 1. Each of the additional sites is on the boundary of either an interlayer tow-tow contact or an intralayer tow-tow contact. As separate solids, the computed geometric entities are meshed with quadratic tetrahedral elements. Mesh deformation techniques are employed subsequently to improve the quality of the assembled mesh, which is incongruent at the tow-intertow matrix and tow-tow interfaces. The interfaces are modeled with the “cohesive contact surface” in Abaqus/Explicit not only to resolve the incongruence but also to simulate progressive interfacial damage. The fabric composite investigated herein has a fiber volume fraction of 40%, a matrix volume fraction of 57.1%, and a void volume fraction of 2.9%. The fiber tows have a fiber volume fraction of 54.8% and a matrix volume fraction of 45.2%.

Material Model for Intertow Matrix

The isotropic elastic behavior of the SiC matrix outside the fiber tows is characterized by its Young's modulus, E_m , and Poisson's ratio, ν_m . The coefficient of thermal expansion is denoted by α_m . The “fixed orthogonal crack” model is chosen to simulate intertow matrix fracture. For this model, the onset of a crack is determined by the criterion of maximum tensile stress, subject to the constraint that the direction of tensile stress is orthogonal to existing cracks at that material point. The direction normal to a newly formed crack is aligned with the maximum tensile stress. Therefore, at most three orthogonal cracks may develop at a material point.

The energy dissipation caused by a crack in the intertow matrix is assumed to be governed by a linear softening traction-separation cohesive law which is defined by the tensile strength, S_m , and density of fracture energy dissipation (energy dissipation per unit area of crack extension), G_m . A “smeared-crack” approach is used by Abaqus/Explicit to implement the orthogonal crack model [14]. Therefore, the softening is converted into a stress-strain relation that has to be adjusted according to the size of the individual finite elements to account for fracture energy dissipation consistently. As a result of the smeared-crack approach, cracks appear in the fashion of strain localization in a numerical solution. General geometric nonlinearity, and the unilateral effect of crack opening and closure are all taken into account in the computation. Properties of SiC in bulk form, as shown below, are used in the present study:

$$E_m = 1.318, \nu_m = 0.14, \alpha_m = 4.5 \times 10^{-6} / ^\circ\text{C}$$

$$S_m = 1.71 \times 10^{-3}, G_m = 6.41 \times 10^{-7}$$

Material Model for Fiber Tows

The present study is not intended to quantitatively predict the overall stress-strain relation. It is known that the process of fiber-matrix debonding influences how fast the internal damage evolves along with the overall stress or strain. It is assumed herein that without reproducing the process of debonding, a sequence of internal damage patterns can be determined, although at what overall stress or strain the patterns appear cannot. As a simple approximation, the fiber tows are represented by a rule-of-mixture model where the reinforcing phase (fiber) is a hypothetical one-dimensional material and assigned the longitudinal Young’s modulus of the carbon fibers, E_f , and coefficient of thermal expansion, α_f . The fiber volume fraction and matrix volume fraction of the tows are denoted by ν_{if} and ν_{im} , respectively. The matrix phase in the rule-of-mixture model can assume transverse isotropy in order to better estimate the phase stress state, and it is also simulated by the smeared-orthogonal-crack approach. The rule-of-mixture model implies a “surrogate” process of fiber-matrix debonding: Upon initiation of a bridged matrix crack at an integration point, debonding starts and completes in no time over the subdivision allotted to the integration point. On the other hand, all the stiffness terms of the carbon fibers other than the longitudinal normal stiffness are low and therefore ignored in the rule-of-mixture model. The simple material model for the fiber tows also implies that the minimum spacing between two bridged matrix cracks in a fiber tow is determined by the longitudinal length of the finite elements of the tow. This minimum spacing may not be physically possible. Therefore, caution should be taken when interpreting numerical results or creating a mesh. As the simplest approximation, the matrix in the rule-of-mixture model is assumed to

be isotropic, and its Young's modulus, E_m , Poisson's ratio, ν_m , coefficient of thermal expansion, α_m , and tensile strength, S_m , are assigned the values identical to those of the intertow matrix. The density of fracture energy dissipation of the matrix in the rule-of-mixture model, G_m , is obtained by applying a reduction factor to G_m . The material constants required to model the fiber tows are listed below:

$$\begin{aligned} \nu_{yf} &= 54.8\%, E_f = 0.740, \alpha_f = -4.1 \times 10^{-7} / ^\circ\text{C} \\ \nu_{im} &= 45.2\%, E_{im} = E_m, \nu_{im} = \nu_m, \alpha_{im} = \alpha_m \\ \nu_{im} S_{im} &= 0.452 S_m, \nu_{im} G_{im} = 0.4 G_m \end{aligned}$$

Material Model for Interfaces

Each interface, either a tow-intertow matrix interface or a tow-tow interface, can be conveniently treated as a pair of cohesive contact surfaces within the Abaqus/Explicit program [14]. The easiest way to define contact surfaces is to define only one for each constituent (tow or intertow matrix) that has all the interfacial element faces of the constituent. Thus, it is also straightforward to create contact pairs. After damage initiates at an interfacial point, the interfacial behavior at that point is represented by a linear softening traction-separation cohesive law. Damage initiates when the ‘‘cohesive-surface quadratic stress criterion’’ variable ($CSQUADSCRT$) reaches one, i.e., $CSQUADSCRT = 1$. $CSQUADSCRT$ is defined by

$$CSQUADSCRT = \sqrt{\left(\frac{\langle t_n \rangle}{t_n^{max}}\right)^2 + \left(\frac{t_s}{t_s^{max}}\right)^2 + \left(\frac{t_t}{t_t^{max}}\right)^2} \quad (1)$$

where t_n , t_s , and t_t denote the three orthogonal traction components acting on an interface, the normal component, first shear component, and second shear component, respectively, and t_n^{max} , t_s^{max} , and t_t^{max} denote the corresponding ultimate strengths. If $t_n < 0$, $\langle t_n \rangle = 0$; if $0 \leq t_n$, $\langle t_n \rangle = t_n$. When damage evolves after the initiation, each mode of the traction-separation response (e.g., normal traction vs. normal separation) follows a softening straight line (as the response envelope) toward the final failure. The area under the envelope for a mode represents the density of fracture energy dissipation due to that mode of damage. The densities of fracture energy dissipation are governed by the following quadratic law:

$$\left(\frac{G_n}{G_n^c}\right)^2 + \left(\frac{G_s}{G_s^c}\right)^2 + \left(\frac{G_t}{G_t^c}\right)^2 = 1 \quad (2)$$

where G_n , G_s , and G_t denote the densities of fracture energy dissipation due to the normal mode, first shear mode, and second shear mode of damage, respectively, in a general damage process, and G_n^c , G_s^c , and G_t^c denote the densities of fracture energy dissipation in the respective pure-mode damage processes. Both the tow-intertow matrix interfaces and tow-tow interfaces are modeled with the same set of material constants. t_n^{max} , t_s^{max} , and t_t^{max} are obtained by applying a common reduction factor to the respective strengths of the SiC intertow matrix based on ultimate tensile strain failure. G_n^c , G_s^c , and G_t^c are obtained by applying respective reduction factors to G_m . The material constants required to model the interfaces are listed below:

$$t_n^{max} = 0.7 S_m, G_n^c = 0.5 G_m$$

$$t_s^{max} = t_t^{max} = 0.7 S_m / (1 + \nu_m), G_s^c = G_t^c = 0.6 G_m$$

The above reduction factors are chosen so as to have the interfaces stronger and tougher than the “smeared” tow matrix, which has strength $\nu_m S_m$ and density of fracture energy dissipation $\nu_m G_m$.

Boundary Conditions

Boundary conditions for remote biaxial normal loading are applied to the boundaries of the finite element model (Figure 1). The bounding surfaces of the porosity are load-free. For convenience, a face of the CMC model is defined as the union of all the flat boundary surfaces that have the same orientation. All the six faces are free of tangential traction. The normal displacement on the $-x$, $-y$, and $-z$ faces is set to zero. The normal displacement on the $+x$, $+y$, and $+z$ faces is constrained to respective master nodes, one on each face. For the stress-controlled biaxial normal loading under consideration, the total normal load on the $+z$ face, applied at the master node on that face, is set to zero, while the total normal loads on the $+x$ and $+y$ faces, applied at the respective master nodes, are prescribed.

NUMERICAL RESULTS AND DISCUSSION

Six load cases, shown in Figure 2, are simulated in this study by specifying the trajectories of the overall stress (composite stress), which is denoted by σ_{ij} with $i, j = x, y, z$. The loading path for each case, as shown in Figure 2, starts from the origin (point 0) and then passes through the other points (points 1, 2, etc.) in the same sequence as the points are numerically marked. All the loading or unloading events are linear segments defined with two consecutively numbered

points. The stress components at the points other than P, Q, and R are either 0, 3.326×10^{-4} , or -3.326×10^{-4} . The stress at P is about 90% of $(\sigma_{xx}, \sigma_{yy}) = (3.326 \times 10^{-4}, 3.326 \times 10^{-4})$, while the stress at Q and R is about 260% of $(\sigma_{xx}, \sigma_{yy}) = (3.326 \times 10^{-4}, 0)$ and about 260% of $(\sigma_{xx}, \sigma_{yy}) = (3.326 \times 10^{-4}, 3.326 \times 10^{-4})$, respectively.

Due to the smeared-crack approach, cracks appear as strain localization in numerical solutions. An estimate of separation strain at the end of linear softening for the intertow matrix, ε_m^* , can be made by using the following equation:

$$\varepsilon_m^* = \frac{2G_m}{S_m L_m} + \alpha_m \Delta T \quad (3)$$

where L_m is the length of subdivisions allotted to the integration points in a typical finite element of the intertow matrix, and ΔT is the temperature difference from the stress-free temperature. Similarly, an estimate of separation strain for the tow matrix, ε_{tm}^* , can be calculated from the following equation:

$$\varepsilon_{tm}^* = \frac{2G_{tm}}{S_{tm} L_t} + \alpha_{tm} \Delta T \quad (4)$$

where L_t is the length of subdivisions allotted to the integration points in a typical finite element of the fiber tows. When plotting contours of the computed maximum principal strain, contours with a value above ε_m^* in the intertow matrix and with a value above ε_{tm}^* in the fiber tows are assigned a gray color. Thus, the pattern of complete separation can be recognized by color easily.

Interfacial damage can be recognized from contour plots of *CSQUADSCRT* on the bounding surfaces of the fiber tows. A series of *CSQUADSCRT* plots generated along a loading path may indicate progression of interfacial damage because once *CSQUADSCRT* reaches unity at any interfacial point (namely, interfacial damage initiates), its value at that location is fixed to one by the analysis code. Therefore, interfacial areas with the maximum value of one, which are colored red in the plots presented below, should monotonically extend.

For the convenience of the description given below, the fiber tows running in the x direction in Figure 1 are called X's and those in the y direction called Y's. The interfaces between the X's and Y's are called X-Y's, those between the X's and intertow matrix called X-M, and those between the Y's and intertow matrix called Y-M's. The different interfaces meet at the boundaries of the X-Y's.

Load Cases 1 and 2

Plots of the maximum principal strain in the intertow matrix and tow matrix, and *CSQUADSCRT* plots on the bounding surfaces of the fiber tows are generated at the points marked for load cases 1 and 2 shown in Figure 2. The plots are presented in Figures 3-6. Before the mechanical loadings start, a 750° C temperature drop is applied to induce an initial stress field in the model. The estimate of separation strain for the intertow matrix from Equation (3) is $\varepsilon_m^* = 0.68\%$, and the estimate for the tow matrix from Equation (4) is $\varepsilon_m^* = 0.56\%$. The results at the end of the thermal loading are marked by point 0 in Figure 3. At point 0, strain concentration is present at the valleys of the intertow matrix void, but it is not severe enough to cause complete separation. On the other hand, limited interfacial damage is seen along the edges of the fiber tows and at the boundaries of the X-Y's when the cool-down ends.

Complete cracking is first seen near the through hole, emanating along the valleys of the intertow matrix void. Later, complete tow matrix cracks (e.g., D_1 in Figures 3 and 5) and intertow matrix cracks (e.g., D_2 in Figures 3 and 5) form on the boundaries of the interlayer tow-tow contacts. These joined cracks are essentially curved, leave a widened damage footprint on the intralayer tow-tow contacts below or above, and cause distributed matrix damage in the tows below or above. The distributed matrix damage induces subsequent intertow matrix cracks (e.g., S in Figures 3 and 5) whose projections onto a fabric plane do not intersect the projections of the driving cracks (e.g., D_1 and D_2 in Figures 3 and 5). No crack initiates from the boundaries of the intralayer tow-tow contacts. This may be attributed to the nearby dominating cracks that originate from the intertow matrix void. The interfacial damage becomes steady at the extreme biaxial tensile load (points 1 and 2 in the load cases 1 and 2, respectively), and the steady interfacial damage on the X-M's and Y-M's are less severe than on the X-Y's.

The pattern of the internal damage caused by load case 1 shows essential 90°-cyclic symmetry, while load case 2 does not induce the cyclic symmetry. Moreover, the major cracks caused by load case 2 are notably different from those by load case 1 in terms of shape. For load case 2, the “older” cracks, which form during the first loading event (from point 0 to point 1), continue to evolve during the second loading event (from point 1 to point 2). Being not orthogonal to the older cracks, the “newer” cracks, which form during the second loading event, appear to be retarded by the evolving older cracks.

Residual crack opening is notable when the model is unloaded, attributed to the initial tensile stress state in the matrix. No damage evolution is observed during the compressive loading events of both load cases. Thus, the plots for the extreme biaxial compressive loading (points 3 and 5 in load cases 1 and 2, respectively) serve as clear images of the severe tensile damage that can filter out. The images suggest that the damage incurred by the extreme biaxial tensile loading of case 1 is more severe than by the extreme biaxial tensile loading of case 2.

The simulations for load cases 1 and 2 conclude that for the plain weave C/SiC composite, the pattern of internal damage strongly depends on the loading path.

Load Cases 3, 4, and 5

It is reported in [12] that uniaxial compressive loading causes evolution of interfacial damage in a typical plain weave CMC whose fiber tows have transverse stiffness greater than that of the intertow matrix. The tows in the C/SiC composite under consideration are more compliant on the transverse plane than the SiC intertow matrix. No damage evolution is observed in the C/SiC composite during the compressive loading events of cases 1 and 2. Load cases 3, 4, and 5 (Figure 2), all with the preceding 750° C temperature drop, are intended to investigate the issue further. Load case 5 is similar to load case 1; however, the unloading in load case 5 starts with significantly less interfacial damage. On the other hand, compressive loading starts immediately from the initial stress state for cases 3 and 4. All the simulations conclude no damage evolution during the uniaxial or biaxial compressive loadings.

Load Case 6

The loading process of case 6 (Figure 2) starts out from the intact material state; it is not preceded by the cool-down. For load case 6, the estimates of separation strain for the intertow matrix and tow matrix from Equations (3) and (4) are $\varepsilon_m^* = 1.02\%$ and $\varepsilon_{tm}^* = 0.90\%$, respectively. In the absence of the initial stress, the applied load levels are elevated in order to generate an extent of damage similar to what is observed in load case 2. The striking effects of the initial stress emerge from a straightforward comparison of Figure 5 with Figure 7. Without the initial stress, the complete cracks are essentially straight, and the “newer” cracks are normal to the “older” cracks, which may lead to weaker interaction between the “newer” and the “older”. Thus, the newer cracks can reach nearly as far as the older cracks, and a pattern of nearly 90°-cyclic symmetry eventually takes shape. The major deviation from the cyclic symmetry is the obviously shorter cracks along the valleys of the intertow matrix void that are essentially parallel with the x axis. These cracks do not start from the through hole; instead, they branch from the older cracks and progress toward the hole as indicated by the arrows in Figure 7.

CONCLUDING REMARKS

For the assumed stacking of the C/SiC plain weaves, the matrix-crack initiation sites are primarily determined by the large intertow matrix voids and interlayer tow-

tow contacts. The numerical results suggest the importance of modeling the geometry and interfacial separation, which is the motive in using the computed geometry and cohesive contact surfaces for the present study. The simulations also conclude that for the plain weave C/SiC composite, the pattern of internal damage strongly depends on the loading path and initial stress.

This paper demonstrates a numerical mesomechanical approach to obtaining the pattern of damage in fabric CMCs, which is useful for formulation of homogeneous continuum models but cannot be easily experimentally determined. Quantitative prediction of the stress-strain relation of fabric CMCs, which is outside the scope of this study, requires a material model that can represent the nonlinear hardening and hysteretic behavior of the fiber tows. Some mesh sensitivity due to the implementation of the smeared crack approach is present in the numerical solutions. To enhance the solution reliability, other more advanced candidates, e.g., extended finite element method, can be employed in future study. Computational time is a challenging issue to the presented numerical solutions. Judicious model reduction may be performed in order to reduce computational time after sufficient characteristics of detailed solutions are known, provided that the ultimate objective is primarily concerned with the effective behavior.

ACKNOWLEDGEMENTS

This paper is based on research funded by the Supersonics Project of the NASA Fundamental Aeronautics Program during 2011 and 2012. The authors are thankful to Mr. David Brewer, who generously shared his expert opinions with the authors during the research and helped revise the manuscript.

REFERENCES

1. Chaboche, J.L., Maire, J.F. (2001). New Progress in Micromechanics-Based CDM Models and their Application to CMCs, *Composites Science and Technology*, 61: 2239–2246.
2. Halm, D., Dragon, A., Charles, Y. (2002). A Modular Damage Model for Quasi-Brittle Solids - Interaction between Initial and Induced Anisotropy, *Archive of Applied Mechanics*, 72: 498–510.
3. Camus, G. (2000). Modelling of the Mechanical Behavior and Damage Processes of Fibrous Ceramic Matrix Composites: Application to a 2-D SiC/SiC, *International Journal of Solids and Structures*, 37: 919–942.
4. Aveston, J., Kelly, A. (1973). Theory of Multiple Fracture of Fibrous Composites, *Journal of Materials Science*, 8: 352–362.
5. Curtin, W.A., Ahn, B.K. Takeda, N. (1998). Modeling Brittle and Tough Stress-Strain Behavior in Unidirectional Ceramic Matrix Composites, *Acta Materialia*, 46(10): 3409–3420.
6. Ismar, H., Streicher, F. (1999). Modelling and Simulation of the Mechanical Behavior of Ceramic Matrix Composites as Shown by the Example of SiC/SiC, *Computational Materials Science*, 16: 17–24.

7. Yang, B., Mall, S. (2003). Cohesive-Shear-Lag Model for Cycling Stress-Strain Behavior of Unidirectional Ceramic Matrix Composites, *International Journal of Damage Mechanics*, 12: 45–64.
8. Murthy, P.L.N., Mital, S.K., DiCarlo, J.A. (1999). Characterizing the Properties of a Woven SiC/SiC Composite Using W-CEMCAN Computer Code, NASA TM–1999-209173.
9. Sullivan, R.M., Murthy, P.L.N., Mital, S.K., Palko, J.L. Cuneo, J.C., Koenig, J.R. (2007). Development of Design Analysis Methods for Carbon Silicon Carbide Composite Structure, *Journal of Composite Materials*, 41(10): 1197–1215.
10. Kuhn, J.L., Haan, S.I., Charalambides, P.G. (2000). Stress Induced Matrix Microcracking in Brittle Matrix Plain Weave Fabric Composites under Uniaxial Tension, *Journal of Composite Materials*, 34(19): 1640–1664.
11. Flores, S., Evans, A.G., Zok F.W., Genet, M., Cox, B., Marshall, D., Sudre, O., Yang, Q. (2010). Treating Matrix Nonlinearity in the Binary Model Formulation for 3D Ceramic Composite Structures, *Composites, Part A*, 41: 222–229.
12. Hsu, S., Cheng, R. (2012). Modeling Geometry and Progressive Interfacial Damage in Textile Composites, *Journal of Composite Materials*, in press.
13. Rao, M.P., Pantiuk, M., Charalambides, P.G. (2011). Modeling the Effects of Stress Concentrations on the Initiation of Matrix Cracking in Woven CMCs, *Journal of Composite Materials*, 45(10): 1121–1143.
14. *Abaqus 6.12 Analysis User's Manual* (2012), Dassault Systèmes Simulia Corporation, Providence, RI.

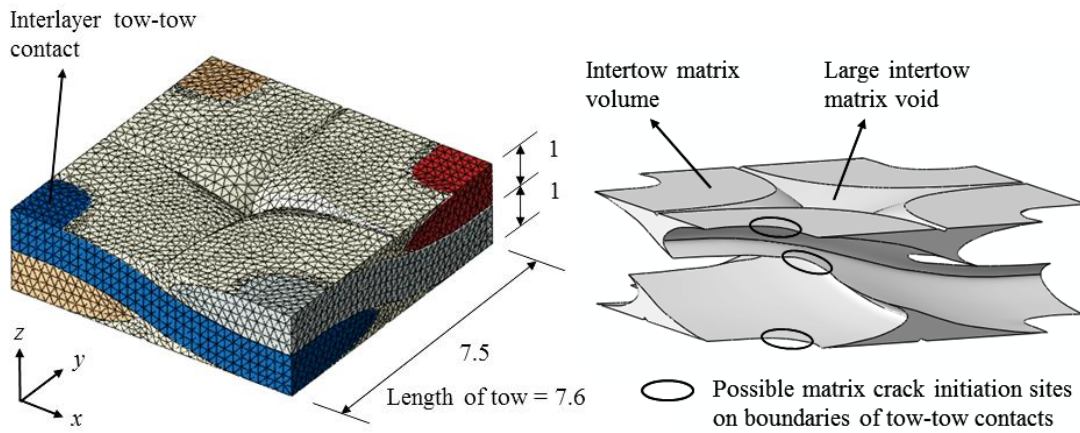


Figure 1. Finite element mesh based on computed in situ geometry and possible matrix-crack initiation sites.

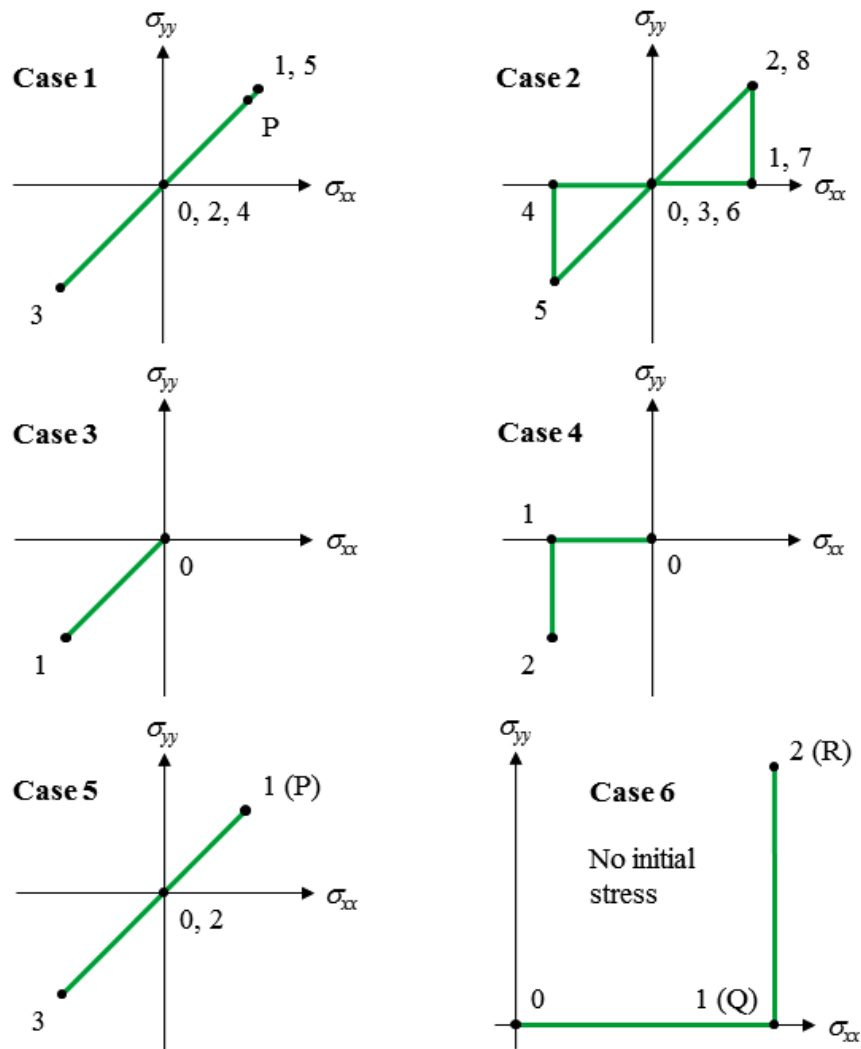


Figure 2. Load cases. Cases 1-5 are preceded by a 750° C cool-down.

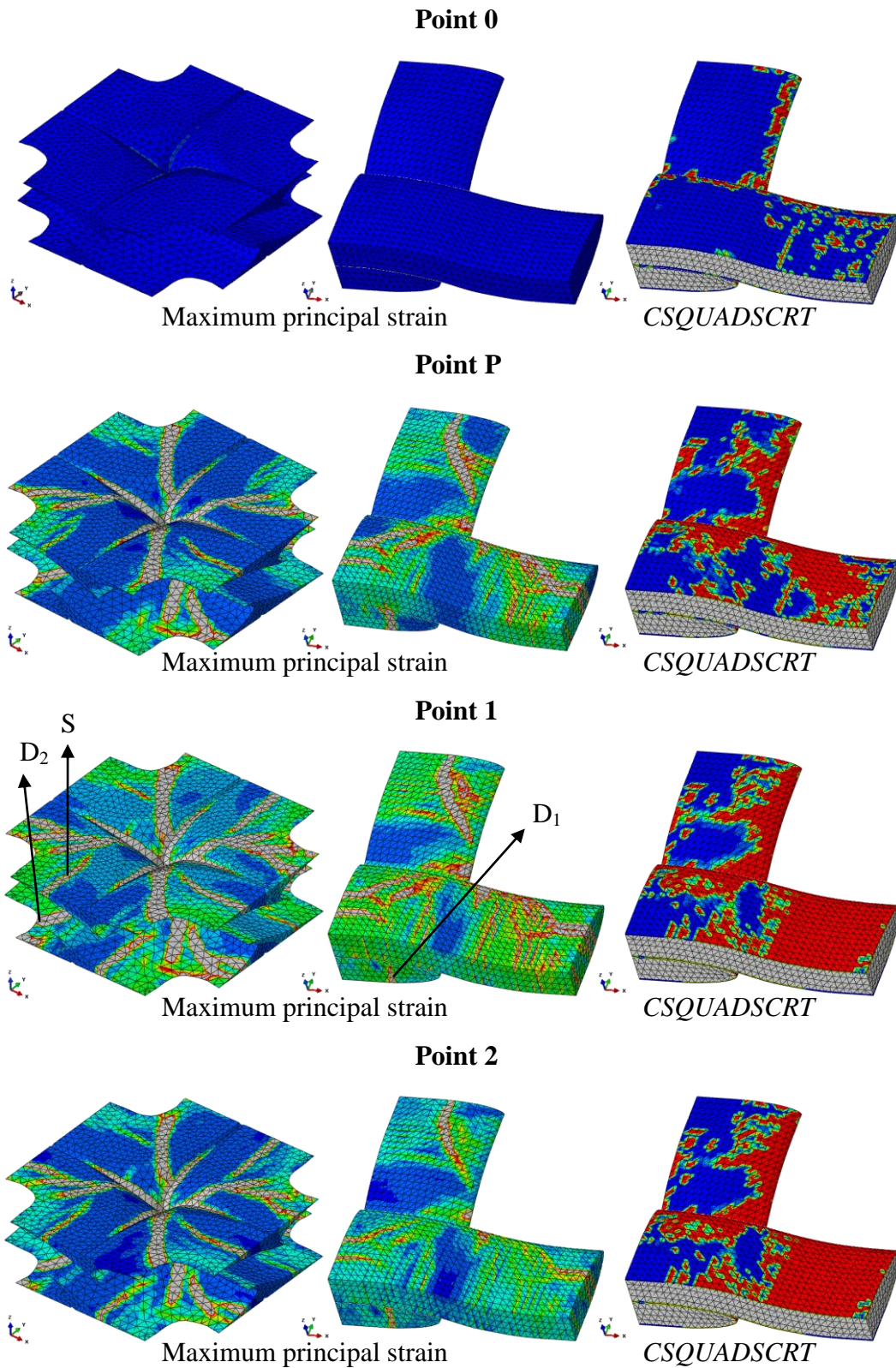
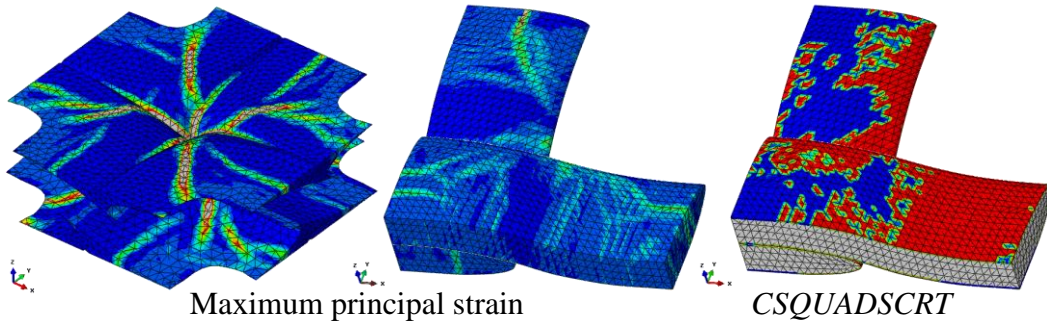
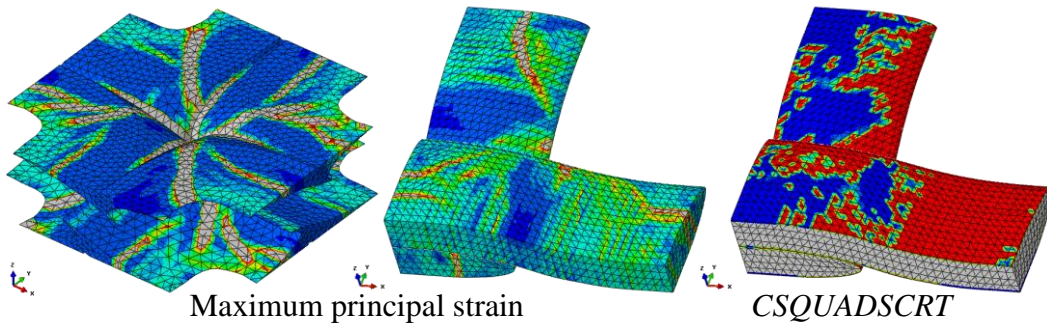


Figure 3. Case 1. Complete-separation regions are colored gray in the maximum principal strain plots. Damage-initiation areas are colored red in the CSQUADSCRT plots.

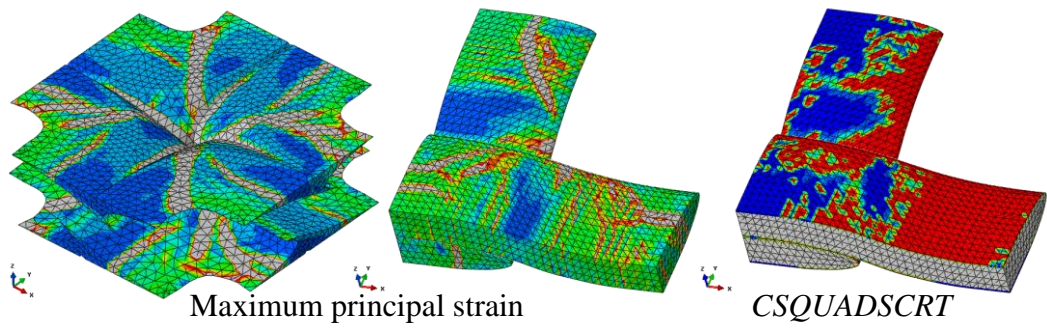
Point 3



Point 4



Point P



Point 5

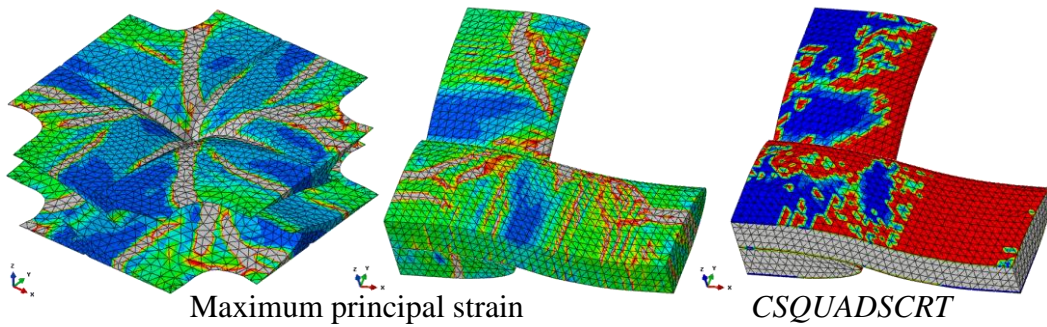


Figure 4. Case 1. Complete-separation regions are colored gray in the maximum principal strain plots. Damage-initiation areas are colored red in the CSQUADSCRT plots.

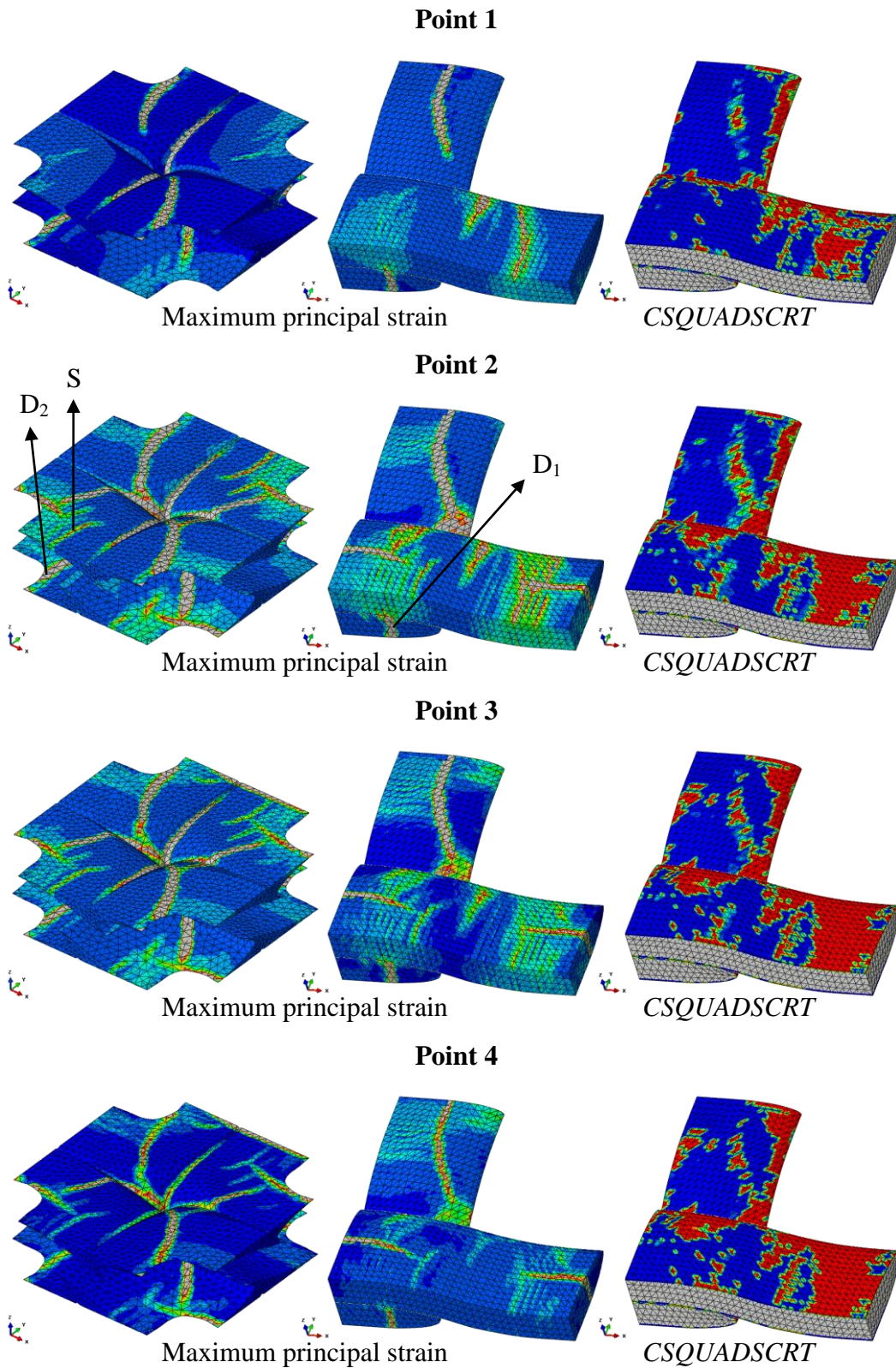
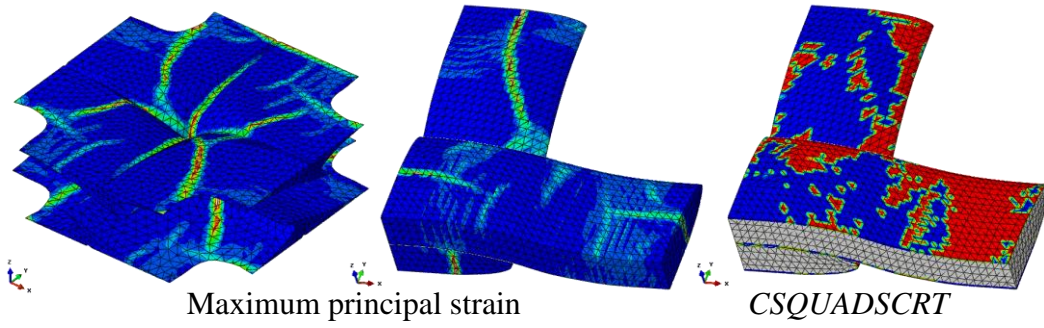
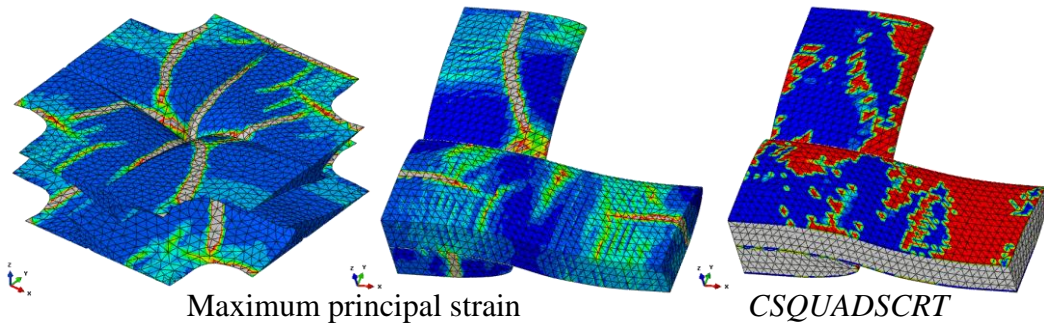


Figure 5. Case 2. Complete-separation regions are colored gray in the maximum principal strain plots. Damage-initiation areas are colored red in the CSQUADSCRT plots.

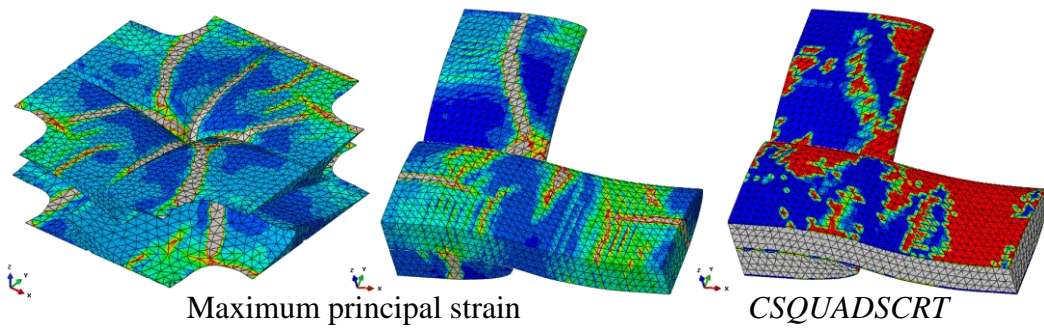
Point 5



Point 6



Point 7



Point 8

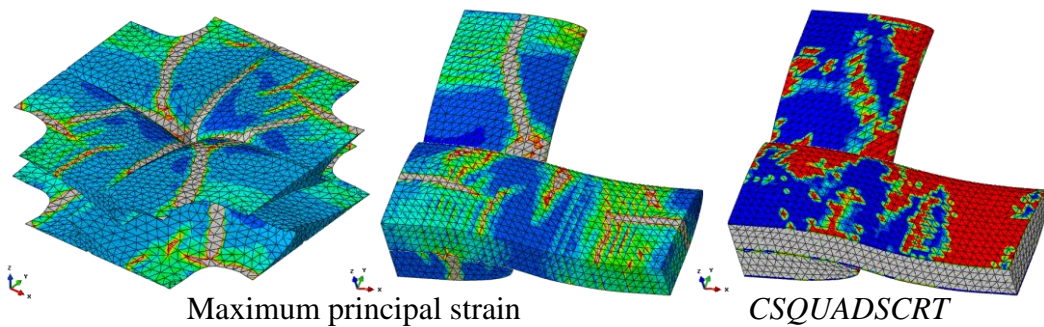
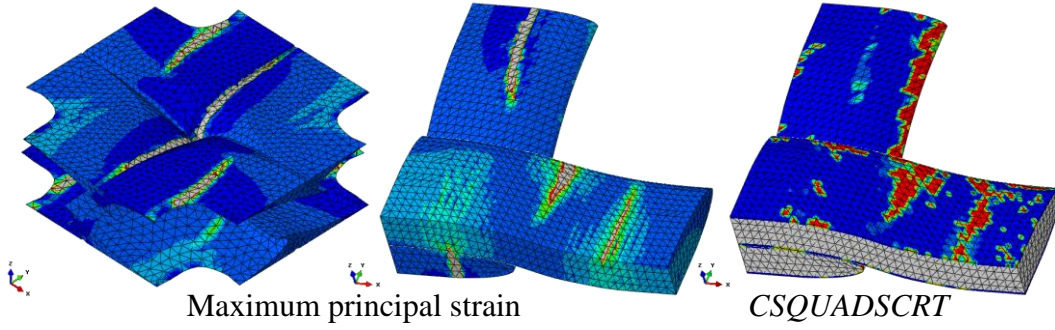


Figure 6. Case 2. Complete-separation regions are colored gray in the maximum principal strain plots. Damage-initiation areas are colored red in the CSQUADSCRT plots.

Point 1 (Q)



Point 2 (R)

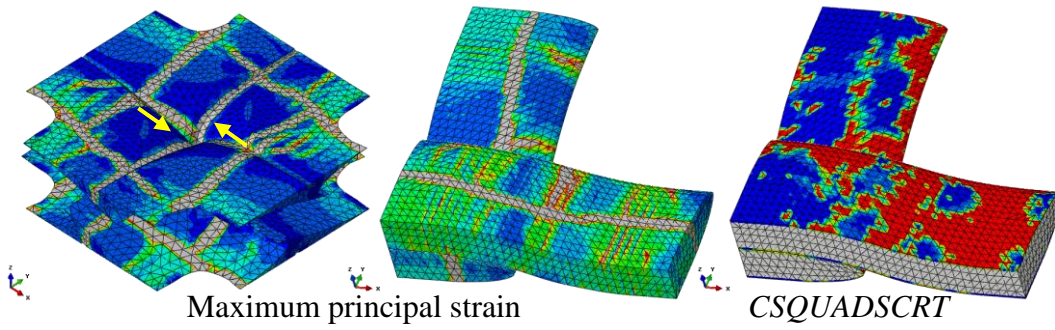


Figure 7. Case 6. Complete-separation regions are colored gray in the maximum principal strain plots. Damage-initiation areas are colored red in the CSQUADSCRT plots.